Vol 18 No 6, June 2009
1674-1056/2009/18(06)/2582-07

Chinese Physics B

© 2009 Chin. Phys. Soc.
and IOP Publishing Ltd

Simulation of magnetization behaviours of Sm(Co,Fe,Cu,Zr)z magnet with low Cu content*

Chen Ren-Jie(陈仁杰)[a)c)†], Zhang Hong-Wei(张宏伟)[b)],
Shen Bao-Gen(沈保根)[b)], Yan A-Ru(闫阿儒)[a)], and Chen Li-Dong(陈立东)[c)]

[a)] *Ningbo Institute of Materials Technology & Engineering, Chinese Academy of Sciences, Ningbo* 315201, *China*
[b)] *State Key Laboratory of Magnetism, Institute of Physics and Center for Condensed Matter Physics, Chinese Academy of Sciences, Beijing* 100190, *China*
[c)] *Shanghai Institute of Ceramics, Chinese Academy of Sciences, Shanghai* 200050, *China*

(Received 17 September 2008; revised manuscript received 28 November 2008)

The effects of microstructure, cell orientation and temperature on magnetic properties and the coercivity mechanism in Sm(Co,Fe,Cu,Zr)z with low Cu content are studied by using the micromagnetic finite element method in this paper. The simulations of the demagnetization behaviours indicate that the pinning effect weakens gradually with the thickness of cell boundary decreasing and strengthens gradually with the cell size decreasing. Because of the intergrain exchange coupling, the coercivity mechanism is determined by the difference in magnetocrystalline anisotropy between the cell phase and the cell boundary phase. And the coercivity mechanism is related to not only the cells alignment but also temperature. With temperature increasing, a transformation of the demagnetization mechanism occurs from the domain pinning to the uniform magnetization reversal mode and the transformation temperature is about 650 K.

Keywords: micromagnetic finite element method, microstructure, cell orientation, temperature
PACC: 7550V, 7560V, 7560G

1. Introduction

The precipitation-hardened Sm(Co,Fe,Cu,Zr)z permanent magnets (PMs) have re-attracted much attention due to their very excellent high temperature magnetic properties since the 1990s.[1−6] These excellent magnetic properties are considered to be related to the complex cellular microstructure, which consists of 2:17 rhombohedral cells each with a size around 100 nm, surrounded by 10 nm 1:5 cell boundaries.[1,7−9] Recently, many research results indicated that the different temperature dependences of coercivity had been discovered in this kind of PM.[1,3−5,10] It is universally received that the coercivity mechanism is controlled by domain wall pinning in this kind of PM, which is determined by the difference in domain wall energy density between the two phases. According to the temperature dependence of coercivity, the Sm(Co,Fe,Cu,Zr)z PMs are distinguished from the traditional Sm(Co,Fe,Cu,Zr)z PMs and the modern Sm(Co,Fe,Cu,Zr)z PMs.[3,10] The coercivity of the former deteriorates rapidly and monotonically with temperature increasing, but the latter exhibits an abnormal temperature dependence of coercivity in a certain temperature range. There are several models to explain the temperature dependence of mechanism of coercivity in Sm(Co,Fe,Cu,Zr)z. And the Cu content in cell boundary phase plays an important role in mechanism and its temperature dependence.[1,3−6,11] If the Cu content in cell boundaries is large enough to make the cell boundary nonmagnetic, the mechanism of coercivity should be controlled by nucleation. But if the Cu content is too low, the cell boundary should be magnetic and the magnetization behaviour becomes very complicated because of the complex microstructure. And thus, the mechanism of coercivity is unclear in Sm(Co,Fe,Cu,Zr)z PMs with low Cu content.

Micromagnetics based on the continuum theory is suitable for the investigation of the magnetization behaviour in a magnet. Recently, the micromagnetic finite-element method (FEM), in which the theory of micromagnetics and the finite-element method combine together, is confirmed to be effective for

*Project supported by the Natural Science Foundation of Zhejiang Province, China (Grant No Y407174).
†Corresponding author. E-mail: chenrj@nimte.ac.cn

the simulation of a magnetization distribution under a magnetic field.[12−15] So, three-dimensional (3D) micromagnetic FEM simulation is usually used to analyse the magnetic behaviour in PMs.[16−21] We have studied the mechanism of magnetization reversal in Sm(Co,Fe,Cu,Zr)z PMs with high Cu content through the micromagnetics FEM simulation.[19−21] In the present paper, the magnetization behaviours of Sm(Co,Fe,Cu,Zr)z PMs with low Cu content are investigated systematically through the micromagnetics FEM simulation using the software package Magpar,[22] and the simulation is described in reference [12]. The effects of microstructure, cells orientation and temperature on magnetic properties and coercivity mechanism are studied in the present paper.

2. The simulation model

According to the continuum micromagnetic theory, the total magnetic Gibbs free energy of a system is composed of the Zeeman energy $\Phi_{\rm H}$, the dipolar energy $\Phi_{\rm D}$, the anisotropic energy $\Phi_{\rm K}$ and the exchange energy $\Phi_{\rm ex}$,[23,24] i.e.,

$$G = \Phi_{\rm H} + \Phi_{\rm D} + \Phi_{\rm K} + \Phi_{\rm ex}. \tag{1}$$

This expression is a function of the direction of the spontaneous polarization $J_{\rm s}$, and the magnetization distribution can be obtained by minimizing the Gibbs free energy. The long-range dipolar–dipolar interaction is solved by introducing a magnetic vector potential. A more detailed description about this method is given in reference [12].

The investigation of the microstructure Sm(Co,Fe,Cu,Zr)z PMs by the transmission electron microscopy reveals that the regular rhombohedral cellular 2:17 phase cell (about 100 nm in size) is surrounded by the 1:5 phase cell boundary (about 10 nm in thickness).[3−5,25,26] Therefore, a cubic model consisting of $5 \times 5 \times 5$ cells is built in the present paper. Figure 1 gives the simulation model. As shown in figure 1, the small cubes represent the Sm_2Co_{17}-type cells, each of which is surrounded by the $SmCo_5$-type cell boundaries. The effects of microstructure and temperature on demagnetization behaviour are studied by simulating the demagnetization process, changing the microstructure parameters (the sizes of cell phase and cell boundary) and magnetic parameters for different temperatures. And the influence of cell alignment degree on demagnetization behaviour is also studied. The mean direction of a sample is fixed on the Z-axis which is parallel to the field direction. And the standard deviation σ is adopted to describe the orientation degree of every cell. And the standard deviation σ is adopted to describe the orientation degree of each cell. A detailed description is given in reference [27].

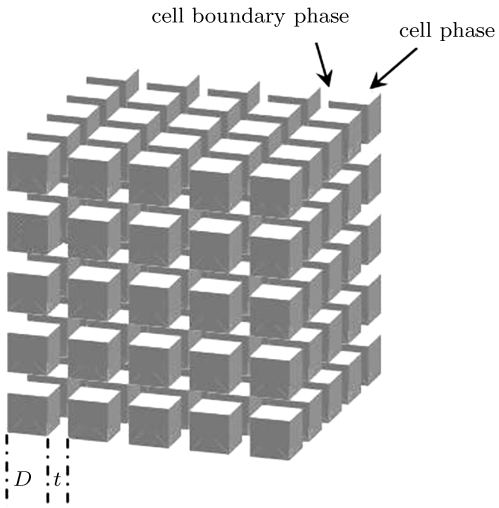


Fig.1. Simulation model composed of 125 cells.

At room temperature (RT), the cell size D varies from 30 nm to 50 nm, with fixing cell boundary thickness $t = 6$ nm, and the cell boundary thickness changes from 2 nm to 8 nm with fixing cell size $D = 50$ nm. The RT magnetic parameters of the cell phase ($J_s^{2:17} = 1.24$ T, $K_1^{2:17} = 2.9$ M·J/m^3, $A^{2:17} = 9.5 \times 10^{-12}$ J/m) and cell boundary phase ($J_s^{1:5} = 0.66$ T, $K_1^{1:5} = 8.1$ M·J/m^3, $A^{1:5} = 7.7 \times 10^{-12}$ J/m) as reported in reference [28] are used in the present simulation. Because of the low Cu content in the cell boundary phase, one can find that the magnetocrystalline anisotropy of the cell boundary is much larger than that of the cell phase. And the saturation magnetization $J_{\rm s}$ of the sample is dependent on the fractions of two phase volumes and related to microstructure as well. The magnetic parameters at high temperatures are deduced through the following equations:

$$\begin{aligned} J_{\rm S}(T) &= C_{\rm J}(1 - T/T_{\rm C})^{\beta}, \\ K_1(T) &= C_{\rm K}(J_{\rm S}(T))^3, \\ A(T) &= C_{\rm A}(J_{\rm S}(T))^2. \end{aligned} \tag{2}$$

Here, $\beta = 0.5$ for the molecular field theory and $\beta = 0.365$ for 3D Heisenberg model. And we adopt the former in this work.

3. Results and discussion

3.1. Influence of microstructure

Figure 2 shows the curves for simulated demagnetization versus coercivity for several cell sizes at RT. In figure 2(a), the cell size D is 50 nm and the cell boundary t changes from 2 nm to 8 nm. The coercivity $\mu_0 H_c$ increases from 2.88 T at $t = 2$ nm to 4.16 T at $t = 8$ nm, but it should not increase obviously when $t \geq 6$ nm. It is contrary to the relationship between coercivity and cell boundary thickness in traditional Sm(Co,Fe,Cu,Zr)z PMs with high Cu content. Because of the low Cu content in cell boundaries, the magnetic anisotropy is stronger in the cell boundaries than that in the cell phase. And the intergrain exchange coupling (IGEC) makes the nucleation field increase in the cell phase, i.e. the cell phase is magnetically hardened by the neighbouring cell boundary phase as done in hard/soft nanocomposite PMs. When the cell boundary thickness t is less than 6 nm, the demagnetization curve shows a single phase PM and no domain wall pinning effect. But a plateau in the demagnetization curve indicates a two-phase demagnetization behaviour and a domain wall pinning process at $t = 8$ nm. Because the anisotropy in the cell boundary is stronger than that in the cell phase, the magnetic reversal starts with the nucleation of a reversal domain in the cell phase and the domain wall is pinned in the cell phase. In the simulation results given by Scholz *et al*,[29,30] the similar phenomenon to the relationship between the effect of domain wall pinning and the thickness of the cell boundary is observed.

Figure 2(b) shows the curves for simulated demagnetization for several cell sizes at cell boundary $t = 6$ nm at RT. The domain wall pinning effect can be observed from all demagnetization curves from $D = 30$ nm to 50 nm. This indicates that the demagnetization processes are controlled by the domain wall pinning. Although the coercivity $\mu_0 H_c$ has almost no change with cell size D decreasing from 50 nm to 35 nm, it increases sharply to 4.97 T when the cell boundary size is 30 nm. It results from two factors: one is the nucleation field increasing due to the IGEC as mentioned above and the other is the relative volume of the IGEC effect v_{ex} increasing with the cell size decreasing. In this paper, the v_{ex} is defined as follows:

$$v_{ex} = \left[\left(D + \delta_B^{1:5}\right)^3 - \left(D - \delta_B^{2:17}\right)^3\right]/(D+t)^3, \quad (3)$$

where $\delta_B^{1:5}$ and $\delta_B^{2:17}$ are the theoretical thicknesses of domain walls in the cell boundary phase and in the cell phase, respectively. Accordingly our simulation results about the microstructure and the impulsive domain wall pinning are related not only to the cell boundary thickness, but also the cell size, i.e. the relative volume v_{ex} of the IGEC effect.

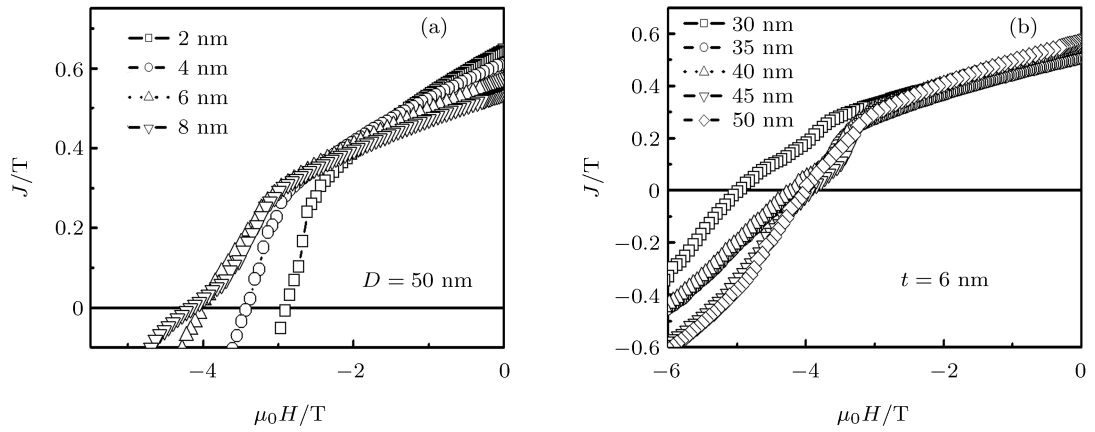


Fig.2. Curves for simulated demagnetization versus coercivity for several different cell boundary sizes (a) and cell sizes (b).

3.2. Influence of cell alignment

In order to study the influence of the cell alignment on demagnetization behaviour, the demagnetization processes are simulated versus orientation distribution of the crystalline anisotropy field in different cells, with different standard deviation degrees of easy axis, i.e. $\sigma = 0°$, $5°$, $10°$, $15°$, $20°$ and $30°$, and 2:17 cell size $D = 50$ nm, and 1:5 cell boundary $t = 6$ nm. The demagnetization curves are shown in figure 3 with the value of σ varying from $0°$ to $30°$ in steps of $5°$.

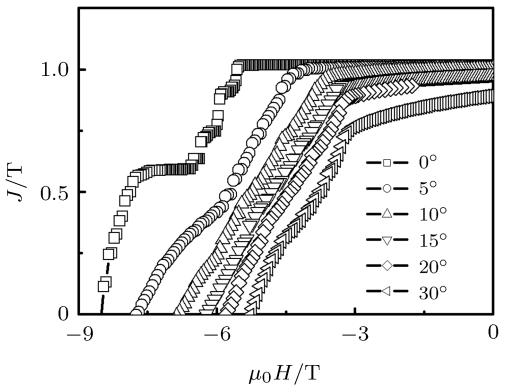


Fig.3. Demagnetization curves for different cell alignment degrees.

For the ideal anisotropic magnet, $\sigma = 0°$ and the demagnetization curve shows an observable plateau at external field $\mu_0 H \approx 6$ T, which is greater than the theoretical nucleation field 5.87 T of the cell phase 2:17 but less than that of the cell boundary phase 1:5. On the one hand, the cell phase is magnetically hardened by the boundary phase which results in the increase of nucleation field. On the other hand, the domain wall is pinned in the boundary phase due to the higher magnetic crystalline anisotropic field than that of the cell. With the deterioration of the cell alignment, the plateau disappears rapidly in the demagnetization curve which indicates that the coercivity mechanism changes from homogeneous pinning to inhomogeneous pinning. It is consistent with our previous simulation results[21] where the coercivity mechanism was related to the crystalline orientation.

Figure 4 shows the curves for remanence ratio m_r, coercivity $\mu_0 H_c$ and maximum energy product $(BH)_{max}$ versus standard deviation σ, and the theoretical m_r in the Stoner–Wohlfarth model is also shown in figure 4(a) for comparison. The value of m_r monotonically decreases with the value of σ increasing, which results from the deviation of magnetic moments from the direction of the external field because of the magnetic crystalline anisotropy in the remanence state. The nucleation field decreases with the deviation from easy axis, which makes the coercivity decrease. According to the simulation results, IGEC leads the value of m_r to be larger than that in the Stoner–Wohlfarth model (the remanence enhancement effect) and the coercivity to be larger than the cell phase nucleation field $\mu_0 H_c = 5.87$ T when $\sigma \leq 15°$ as shown in figure 4(a). Because the value of $\mu_0 H_c$ is much larger than $J_r/2$, the value of $(BH)_{max}$ is determined by the J_r and the dependence of energy product on σ is similar to that of m_r on σ (figure 4(b)). In addition, the squareness of the demagnetization curve deteriorates with the value of σ increasing as shown in figure 3, which makes the value of $(BH)_{max}$ decrease too. Obviously, the cell alignment optimization is an effective way to improve the magnetic properties of PMs.

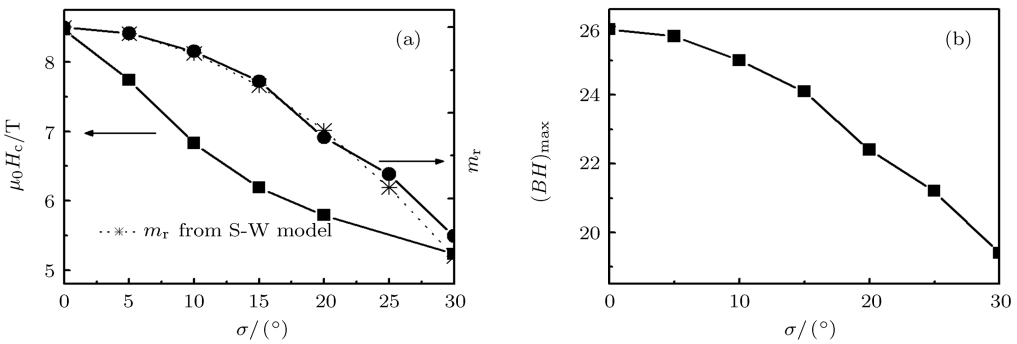


Fig.4. Remanence ratio m_r, coercivity $\mu_0 H_c$ (a) and maximum energy product $(BH)_{max}$ (b) versus standard deviation σ.

4. Simulations of demagnetization at different temperatures

Figures 5(a) and 5(b) show the demagnetization curves of anisotropic and isotropic magnets at different temperatures for $D = 50$ nm and $t = 6$ nm, respectively. For anisotropic magnet, the demagnetization curves each have a plateau at lower temperatures. This phenomenon is caused by the fact that the domain wall homogeneous pinning effect gradually weakens with temperature T increasing and even disappears at $T > 500$ K as shown in figure 5(a). However, no plateau can be observed in the whole temperature range under study for isotropic magnet as shown in figure 5(b). And comparing figure 5(a) with figure 5(b), one can find that the nucleation field of the anisotropic sample is much larger than the coercivity of isotropic sample at the same temperature. It maybe indicates that the coercivity mechanism is controlled by inhomogeneous domain wall pinning or magnetic moment reversal in the isotropic sample. As mentioned above, the coercivity mechanism is related to the crystalline orientation. In the isotropic sample, the depinning fields of the cells with different orientations are different, or even the progress of demagnetization is totally controlled by the magnetic moment reversal in some cells. This leads the plateau to disappear in the demagnetization curve as shown in figure 5(b).

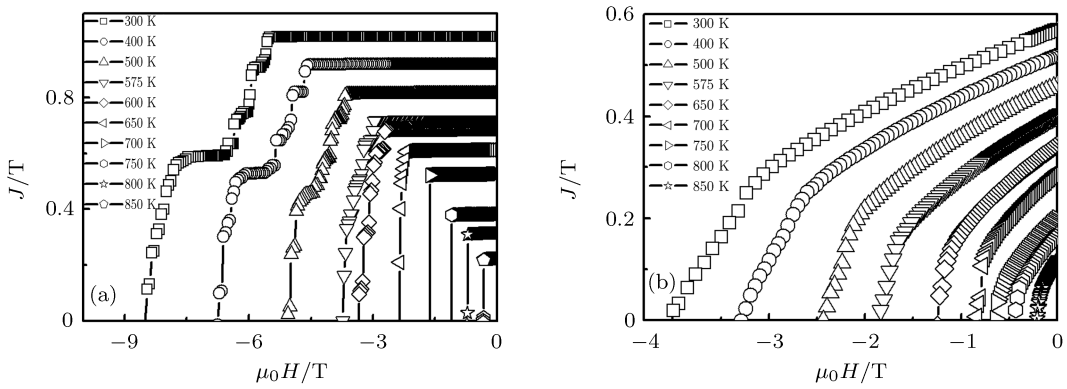


Fig.5. Demagnetization curves for anisotropic (a) and isotropic samples (b) at different temperatures.

According to the theory of domain wall pinning,[5,11,31,32] the coercivity mechanism should change from the repulsive model to the attractive model, if the domain wall energy density of 1:5 cell boundary phase $\gamma_{1:5}$ changes from larger to less than that of 2:17 cell phase $\gamma_{2:17}$ with temperature increasing. At the critical transition temperature (about 575 K in this work), $\gamma_{1:5}$ is equal to $\gamma_{2:17}$ and the domain walls undergo a motion subject to no resistance. But the domain wall pinning can be observed in the demagnetization curve at $T = 575$ K and the pinning effect disappears at $T = 650$ K as shown in figure 5(a). Obviously, the demagnetization mechanism becomes of uniform rotation model when temperature is higher than 650 K in which range the magnetocrystalline anisotropy constant of the cell phase $K_1^{2:17}$ is very close to that of the cell boundary phase $K_1^{1:5}$. That indicates that the pinning field is determined by the difference in magnetocrystalline anisotropy ΔK_1 between the cell phase and the cell boundary phase. At $T > 650$ K, $\Delta K_1 < 0.4 \times 10^6$ J/m^3, the demagnetization process is controlled by the uniform rotation in the cell phase and the pinning effect disappears as shown in figure 5(a). Similar phenomena were reported by Scholz *et al.*[29,30]

Figure 6 shows the magnetization distributions in the demagnetization process for the anisotropic sample at 500 K. The magnetization reversal occurs in the centres of the cells firstly due to the action of lower anisotropic field. And the outer moments of the cells keep in their magnetization states even when the external field increases to 4.85 T (1.235 times the anisotropic field of the cell phase) as shown in figure6 (a), which is due to the magnetic hardening effect coming from the cell boundary phase. With external field increasing, these demagnetization nucleations propagate and the magnetization areas are compressed and then the domain walls move into the cell boundary phase but are pinned at the cell boundary, which results in the plateaus of the demagnetization curves as shown in figure 5(a). With external field further increasing, the magnetic moments of the cell boundary phase further cause the reversal and only the moments in the corners of the cell boundaries keep in their magnetization states when the external field reaches to 8.27 T (see figure 6(d)). Obviously, in the

demagnetization process the magnetization reversal mechanism is controlled by the domain wall pinning at the cell boundary according to the magnetization distribution in the demagnetization process.

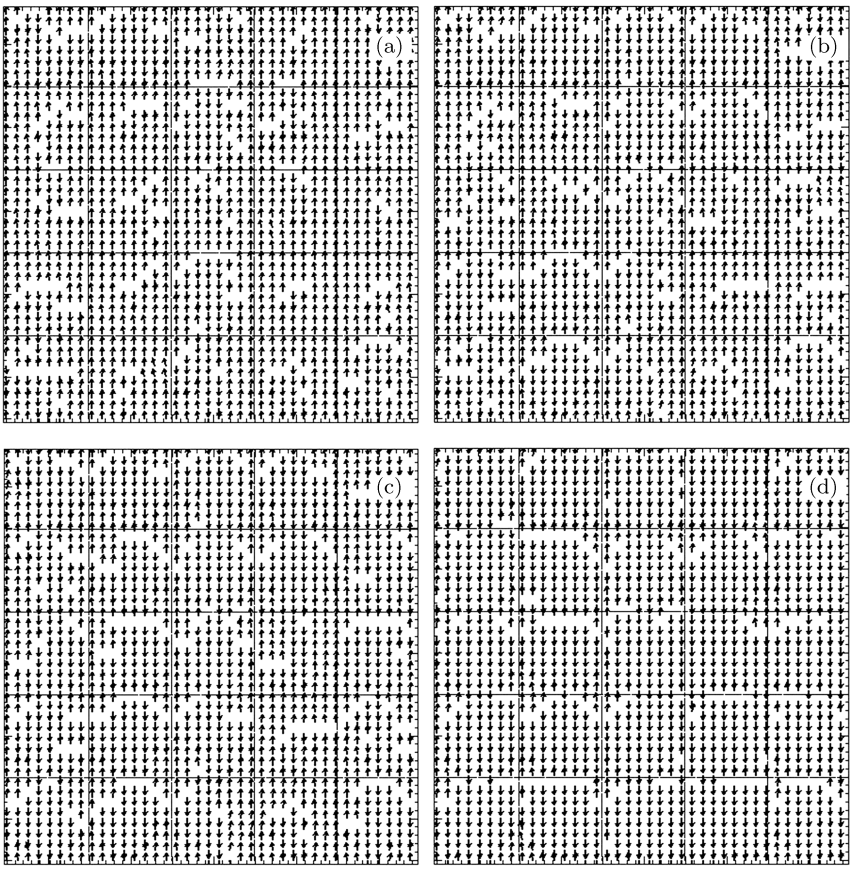


Fig.6. Magnetization distributions in demagnetization process for anisotropic sample at 500 K under external fields of 4.85 T (a), 5.05 T (b), 5.17 T (c) 8.27 T (d) separately.

5. Conclusion

The effects of microstructure, cells orientation and temperature on magnetic properties and coercivity mechanism in Sm(Co,Fe,Cu,Zr)z with low Cu content are studied by using the micromagnetic FEM. Because the magnetocrystalline anisotropy of the cell boundary phase is stronger than that of the cell phase at RT, the pinning effect weakens gradually with the thickness of cell boundary decreasing, and strengthens gradually with the cell size decreasing. The IGEC leads the magnetic moments of the cell phase to be hardened and the coercivity to be higher than the theoretical nucleation field of the cell phase. The study of the cells alignment influence indicates that the coercivity mechanism is related to the cell alignment and the magnetic properties deteriorate with σ increasing. Because of the IGEC, the coercivity mechanism is determined by the difference in magnetocrystalline anisotropy ΔK_1 rather than the difference in domain wall energy density $\Delta\gamma$ between the cell phase and the cell boundary phase. With the increase of temperature, a transformation of the demagnetization mechanism occurs from the domain pinning to the uniform magnetization reversal mode and the transformation temperature is about 650 K in this work.

References

[1] Popov A G, Korolev A V and Shchegoleva N N 1990 *Phys. Met. Metall.* **60** 100

[2] Liu J F, Ding Y and Hadjipanayis G C 1999 *J. Appl. Phys.* **85** 1670

[3] Hadjipanayis G C, Tang W, Zhang Y, Chui S T, Liu J F, Chen C and Kronmüller H 2000 *IEEE Trans. on Magn.*

36 3382
[4] Goll D, Kleinschroth I, Sigle W and Kronmüller H 2000 *Appl. Phys. Lett.* **76** 1054
[5] Zhou J, Shomski R, Chen C, Hadjipanayis G C and Sellmyer D J 2000 *Appl. Phys. Lett.* **77** 1514
[6] Gabay A M, Tang W, Zhang Y and Hadjipanayis G C 2001 *Appl. Phys. Lett.* **78** 1595
[7] Tang W, Zhang Y and Hadjpanayis G C 2000 *IEEE Trans. on Magn.* **36** 3294
[8] Zhang Y, Tang W, Hadjpanayis G C, Chen C, Nelson C and Krishnan K 2001 *IEEE Trans. on Magn.* **37** 2525
[9] Chen X, Liu J F, Ni C, Hadjipanayis G C and Kim A 1998 *J. Appl. Phys.* **83** 7139
[10] Liu J F, Chui T, Dimitrov D and Hadjipanayis G C 1998 *Appl. Phys. Lett.* **73** 3007
[11] Chui S T 2000 *J. Magn. Magn. Mater.* **217** 120
[12] Schrefl T, Fidler J and Kronmüller H 1994 *J. Magn. Magn. Mater.* **138** 15
[13] Fischer R and Kronmüller H 1996 *Phys. Rev.* B. **54** 7284
[14] Fischer R, Leineweber T and Kronmüller H 1998 *Phys. Rev.* B **57** 10723
[15] Zhang H W, Rong C B, Du X B, Zhang J, Zhang S Y and Shen B G 2003 *Appl. Phys. Lett.* **82** 4098
[16] Rong C B, Zhang H W, Zhang J, Du X B, Zhang S Y and Shen B G 2004 *J. Appl. Phys.* **95** 1351
[17] Rong C B, Zhang H W, Du X B, Zhang J, Zhang S Y and Shen B G 2004 *J. Magn. Magn. Mater.* **277** 221
[18] He S L, Zhang H W, Rong C B, Chen R J and Shen B G 2005 *Chin. Phys.* **14** 1055
[19] Chen R J, Rong C B, Zhang H W, He S L, Zhang S Y and Shen B G 2004 *Acta Phys. Sin.* **53** 4341 (in Chinese)
[20] Chen R J, Zhang H W, Rong C B, Sun J R and Shen B G 2006 *J. Magn. Magn. Mater.* **305** 191
[21] Chen R J, Zhang H W, Rong C B, Sun J R and Shen B G 2006 *J. Appl. Phys.* **100** 043901
[22] Scholz W, Fidler J, Schrefl T, Suess D, Dittrich R, Forster H and Tsiantos V 2003 *Comp. Mat. Sci.* **28** 366
[23] Brown W F Jr 1963 *Micromagnetics* (New York: Wiley-Interscience)
[24] Schrefl T, Fidler J and Kronmüller H 1994 *Phys. Rev.* B **49** 6100
[25] Liu S, Yang J, Doyle G, Kuhl E, Chen C H, Walmer M S and Simon G 1999 *IEEE Trans. on Magn.* **35** 3325
[26] Liu S, Yang G, Goyle G, Potts G and Kuhl G E 2000 *J. Appl. Phys.* **87** 6728
[27] He S L, Zhang H W, Rong C B, Chen R J, Sun J R and Shen B G 2005 *Acta Phys. Sin.* **54** 3408 (in Chinese)
[28] Goll D, Müller K H, and Stadelmaier H H 2004 *J. Appl. Phys.* **96** 6534
[29] Scholz W, Fidler J, Schrefl T, Suess D and Matthias T 2002 *J. Magn. Magn. Mater.* **242-245** 1356
[30] Scholz W, Fidler J, Schrefl T, Suess D and Matthias T 2002 *J. Appl. Phys.* **91** 8492
[31] Livingston J D and Martin D L 1977 *J. Appl. Phys.* **48** 1350
[32] Nagel H 1979 *J. Appl. Phys.* **50** 1026